Updated BAND Simulation

Axel Schmidt

February 13, 2017

1 Introduction

The design of the BAND detector has been significantly refined since its original proposal [1], and correspondingly updated simulation is needed. I have begun work on such a simulation, and in this report I present the current results. These results will naturally be refined and improved as the simulation becomes more sophisticated and as the detector design solidifies. This report is only meant to update the estimates from the proposal and showcase the current status.

The original source of this simulation software is the generator written by Wim and Or, which was used to produce numbers for the proposal. I have reorganized the code in several ways, while leaving Wim's cross section calculation unchanged. The code now uses the `CMake` build system so that it is easily compilable across platforms. The generators now use ROOT's `TFoam` class to generate events continuously over the supplied probability distribution. Version control is managed with `git`. The entire repository can be downloaded from:

`https://github.mit.edu/schmidta/deuteron_dis`

2 Assumptions

For the simulation studies in this report, I use the following assumptions:

- e^- generation range: 5°–35° in θ, 2–8 GeV/c in $|\vec{p}|$
- n generation range: 160°–170° in θ, 275–600 MeV/c in $|\vec{p}|$
- 40 day run period
- Instantaneous luminosity (per nucleus) of 10^{35} cm^{-2}s^{-1}
- 50% azimuthal coverage for detecting the electron in CLAS12
- 60% azimuthal coverage for detecting the neutron in BAND
- 30% detection efficiency for neutrons in BAND

Furthermore, I require that events of interest meet the following criteria:

- Reconstructed $Q^2 > 2$ [GeV/c]^2
- Reconstructed $W' > 1.8$ GeV
- The reconstructed angle between the neutron and momentum transfer vector, θ_{rq}, $> 110°$.

For some studies, I had to make assumptions about the geometry of BAND. In this report, I always assumed that the BAND scintillators extended from 2.9 m to 2.5 m upstream of the center of the target. I assumed that the speed of light in the BAND scintillator plastic was 15 cm/ns (an index of refraction $n_{\text{scint.}}$ of approximately 2). The width of scintillator bars was a parameter in the detector simulation. A hit in a

scintillator bar was assumed to be reconstructed along the center of the bar. For reconstruction of position along the length of a bar, I related the resolution σ_x to the PMT time resolution σ_t according to:

$$\sigma_x = \frac{c\sigma_t}{n_{\text{scint.}}\sqrt{2}}. \tag{1}$$

Similarly, momentum was reconstructed from the flight time of the neutron, smeared with a resolution

$$\sigma_T = \frac{\sigma_t}{\sqrt{2}}. \tag{2}$$

The time resolution of a PMT was assumed to be constant regardless of the hit position along the length of the bar. We know that this is a bad assumption, but haven't yet developed a better model.

2.1 CLAS12 Resolutions

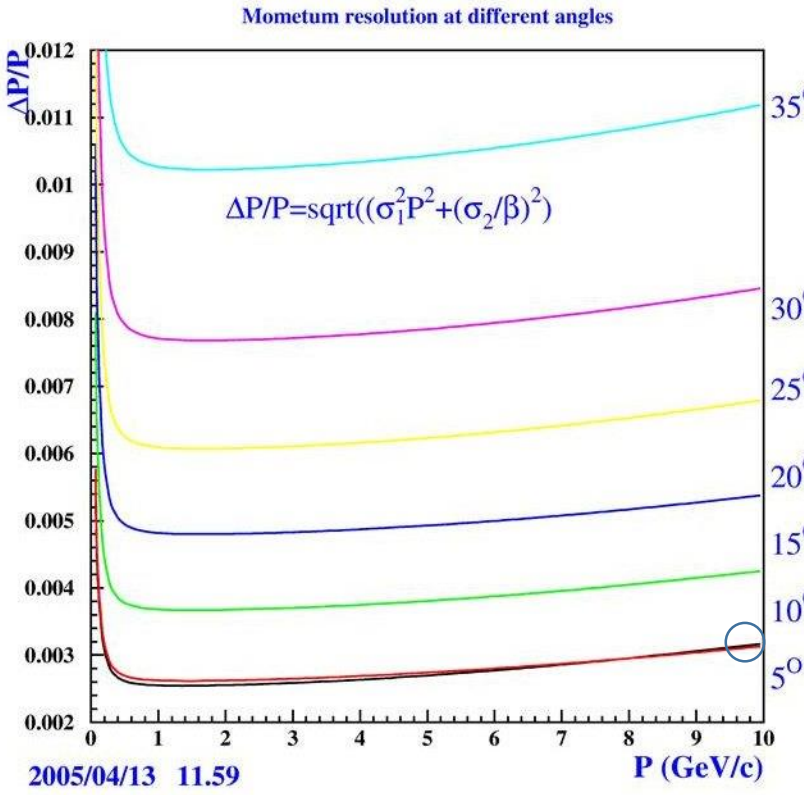

Figure 1: The estimated best-case scenario for the CLAS12 momentum resolution

The CLAS12 spectrometer has non-zero resolution for reconstructing the scattered electron, and I need to make some assumptions about the CLAS12 performance. For the angular resolutions, I follow the CLAS12 drift chamber group's website[2]: I use 1 mrad for θ, and 1 mrad/$\sin\theta$ for ϕ. The momentum resolution of CLAS12 is expected to depend weakly on momentum (over the 2–8 GeV range) but strongly on the scattering angle (see figure 1). For the sake of simplicity, I have chosen to ignore the momentum-dependence on the resolution, and to make a simple model of the angular dependence:

$$\Delta p/p = A + B\sin\theta + C\cos\theta. \tag{3}$$

I fit the coefficients A, B, and C to the approximate resolutions for $p = 5$ GeV/c electrons from figure 1.

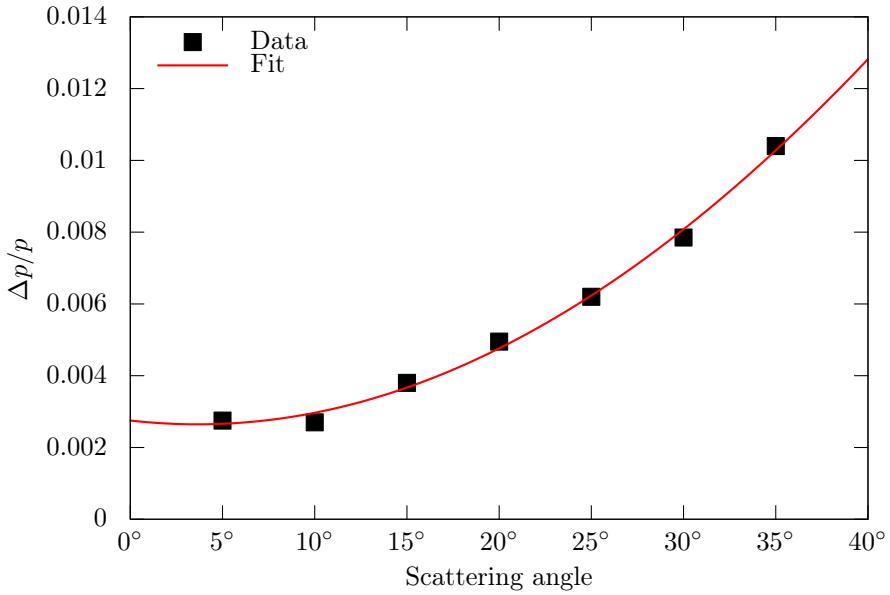

Figure 2: I modeled the angular dependence of the momentum resolution with a simple equation given in eq. 3.

The data and the resulting fit are shown in figure 2. The best fit values of the coefficients are:

$$A = 0.0549141$$
$$B = -0.00332126$$
$$C = -0.052163$$

I will show results with three different CLAS12 resolutions. The resolutions as described above will be referred to "normal resolutions." I will also show results with the resolution estimates doubled, which I will refer to as "double resolutions." Lastly, I will show results in which the CLAS12 reconstruction is unsmeared, which I will refer to as "perfect resolution."

3 Distributions

In this section, I show several kinematic distributions for events of interest. In these plots, I use the following smearing procedure for neutron reconstruction in BAND:

- 200 ps PMT resolution,
- Scintillator bars with a 7×7 cm^2 square profile.

The reconstructed electron kinematics are smeared according to the normal resolution of subsection 2.1. Figure 3 shows the reconstructed electron momentum vectors. Figure 4 shows the reconstructed neutron momentum relative to the momentum transfer vector $\vec{q}$. Figure 5 shows the distribution of events in Q^2 and x'. While all three of these plots show distributions of smeared reconstructed variables, there is little visible difference compared to unsmeared distributions, when viewed as color-map plots.

4 Rate and Background Estimates

Random coincidences of scattered electron events and backward going neutrons can fake $(e, e'n)$ events of interest. To estimate the rate of this random background, two cross sections are needed; the inclusive (e, e') cross section, and the cross section for neutron production. For the former, I use Wim's inclusive cross

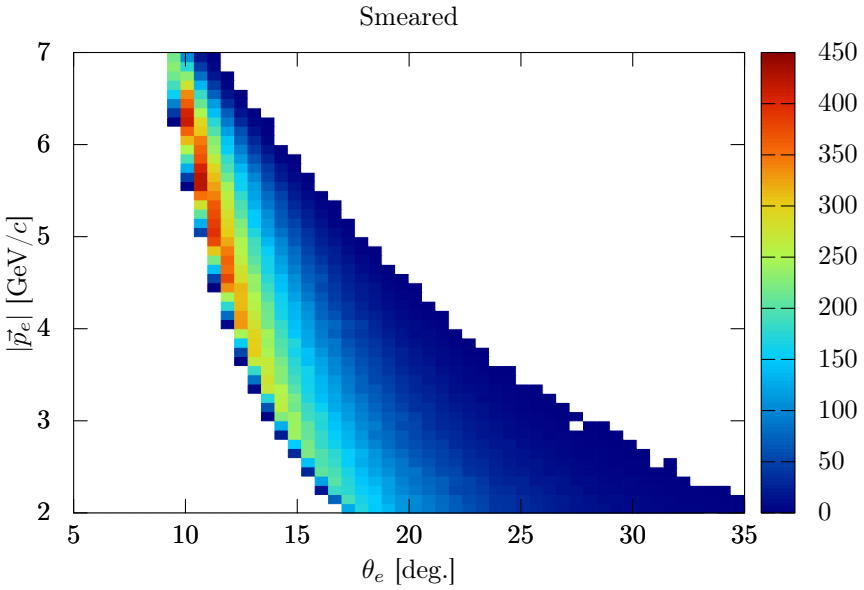

Figure 3: The distribution of reconstructed electron momentum vectors

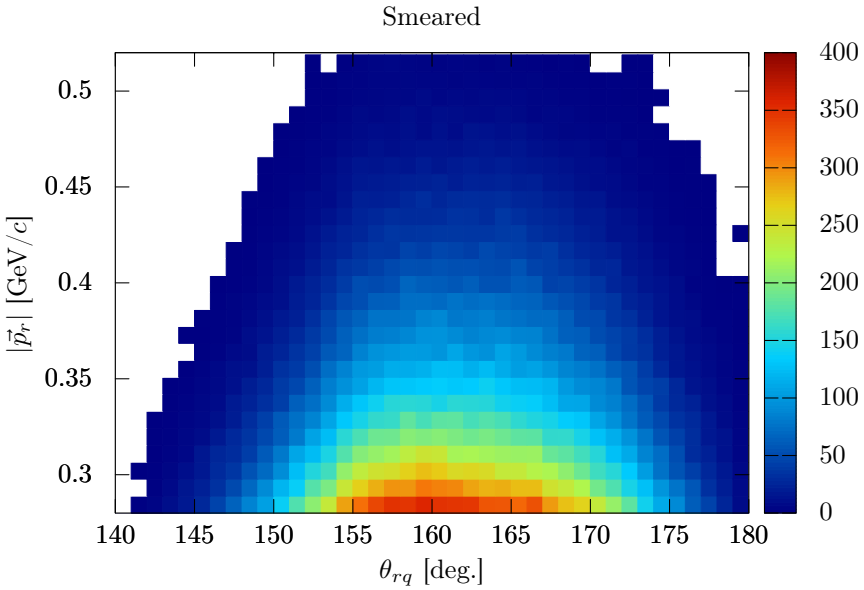

Figure 4: The distribution of reconstructed neutron momentum vectors

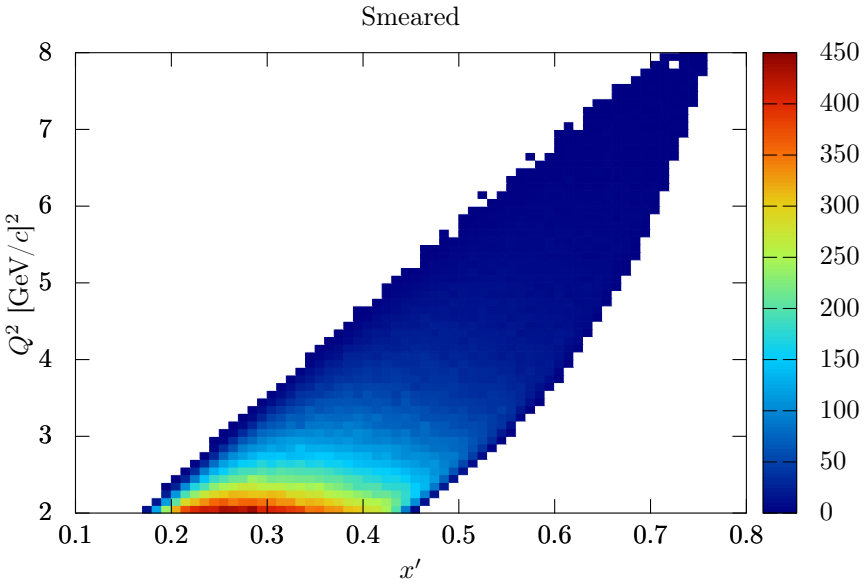

Figure 5: The distribution of reconstructed x' and Q^2 of events of interest

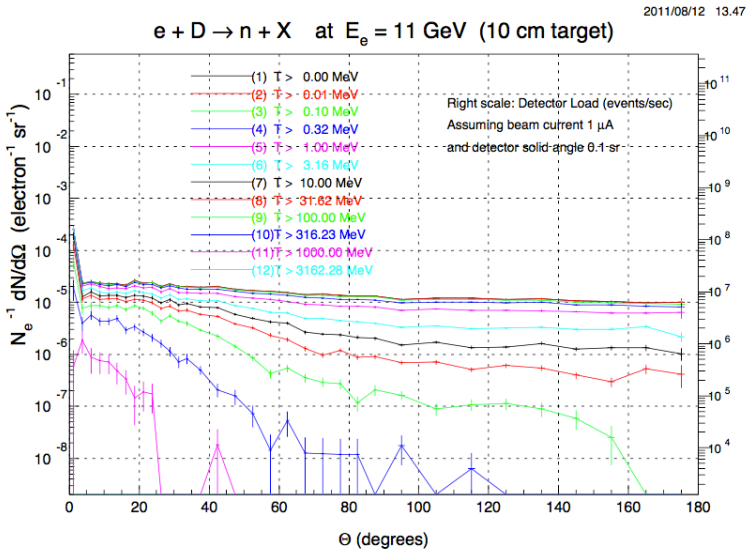

Figure 6: Calculations of the single neutron flux for energies (figure B2 from [1])

section code. For the latter, I follow the estimates of Appendix B of the BAND proposal [1]. In the proposal, calculations by Pavel Degtiarenko of the single neutron flux (shown in figure 6) produced by an electron beam on a deuterium target are used to estimate the expected rates in BAND. I use the same numbers as the BAND proposal for the same of consistency: the rate of neutrons with kinetic energy greater than 15 MeV (enough to produce a signal above threshold in the BAND scintillators) are produced isotropically at a rate of 4×10^5 s^{-1} through a 0.1 sr detector at a luminosity of 6×10^{36} cm$^{-2}s^{-1}$. This is equivalent to a differential cross section of:

$$\frac{d\sigma}{d\Omega} = \frac{R}{L\Omega} \tag{4}$$

$$= \frac{4 \times 10^5 \mathrm{cm}^2\mathrm{s}}{\mathrm{s} \times 0.1\mathrm{sr} \times 6 \times 10^{36}} \tag{5}$$

$$= 6.667 \times 10^{-31}\mathrm{cm}^2/\mathrm{sr} = 666.7\mathrm{nb/sr} \tag{6}$$

The arrival time probability of a random single neutron is constant in time. Since neutron momenta are inferred from flight time relative to the lepton vertex time, the random neutrons will appear to have a specific momentum distribution (see figure 11.) The inferred neutron momentum is given by:

$$p_r = \frac{m_N}{\sqrt{\frac{(t_{\mathrm{hit}} - t_{\mathrm{vertex}})^2 c^2}{z^2} - 1}}, \tag{7}$$

where z is the flight distance between the target and BAND (2.5 m). The hit time t_{hit} is a uniformly distributed random variable.

The minimum and maximum momenta of interest determine the minimum and maximum flight time and thus define the coincidence window, Δt_{co}, in which random neutrons appear as signal. Inverting equation 7, we get

$$(t_{\mathrm{hit}} - t_{\mathrm{vertex}}) = \frac{z}{c}\sqrt{1 + \frac{m_N^2}{p_r^2}}, \tag{8}$$

defining the time window:

$$\Delta t_{\mathrm{co}} = \frac{z}{c}\left(\sqrt{1 + \frac{m_N^2}{p_{\mathrm{min.}}^2}} - \sqrt{1 + \frac{m_N^2}{p_{\mathrm{max.}}^2}}\right). \tag{9}$$

For the background estimates in this report, I considered neutrons with momenta between 275 and 700 MeV, which yields a time window Δt_{co} of 15.7 ns.

The number of random background events in a run of length T, with luminosity L is thus given by:

$$dN = \frac{d\sigma}{d\Omega}_e d\Omega_e \frac{d\sigma}{d\Omega}_n d\Omega_n L^2 T \Delta t_{\mathrm{co}}. \tag{10}$$

Figure 7 shows the distribution of all random coincidence events (regardless of W' and Q^2 cuts) as functions of reconstructed flight time and of the inverse of the reconstructued momentum. Note these values are unrelated to the true flight time and momentum of the neutron contributing the to random coincidence. Instead, these quantities are (falsely) inferred from the neutron hit time relative to the electron detected in CLAS12. For random coincidences, the flight time should be uniformly distributed (up to acceptance edges) and this is confirmed in simulation. The inverse-momentum distribution should also be uniformly distributed in the non-relativistic limit. The simulated distribution is uniform on the right (the low-momentum, non-relativistic edge), and tails off on the high-momentum left edge, exactly as expected.

Figure 8 shows the distribution of signal (black line) and background (gray shading) events binned in x'. At low x', signal exceeds the background, but at larger x', the background rate is greater than the signal rate. Figures 9, 10, 11, 12, 13 show the distributions of events segregated in two x' regimes. The red plots on the left show events for $0.25 < x' < 0.35$, while the blue plots on the right, $x' > 0.5$.

The background-to-signal ratio is shown in figure 14. (Compare to figure B4 of the proposal). For the low x' kinematics, the background only amounts to approximately 40% of the signal in the α_s region of interest. This is slightly more favorable than the scenario presented inthe proposal. For the high x' kinematics, the background exceeds the signal by nearly a factor of two in some bins. This is slightly worse than the scenario presented in the proposal. The differences between the estimate presented here and the proposal are driven largely by the reduction of the W' limit from 2 GeV in the proposal down to 1.8 GeV in this report.

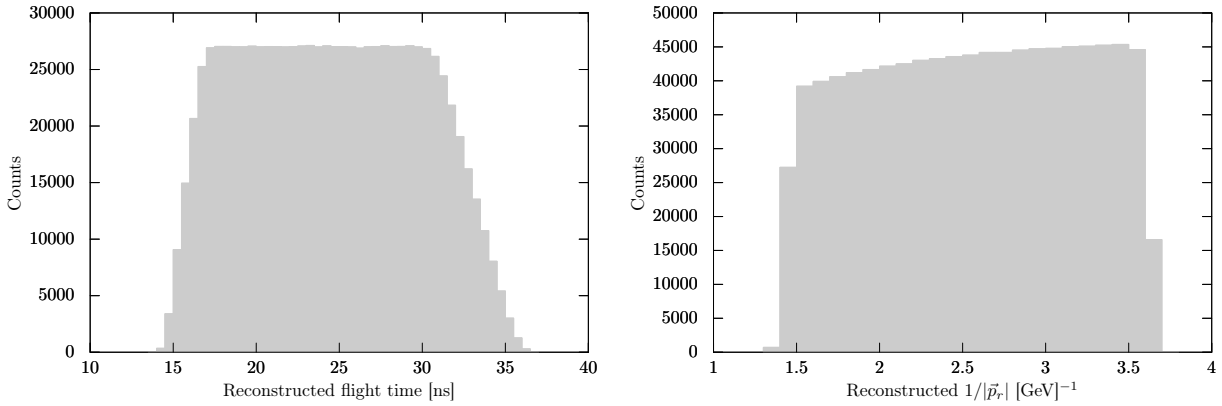

Figure 7: The distribution of random background events are shown as a function of reconstructed flight time (left) and of the inverse of the reconstructed momentum (right). These distributions confirm that the simulated background behaves as expected.

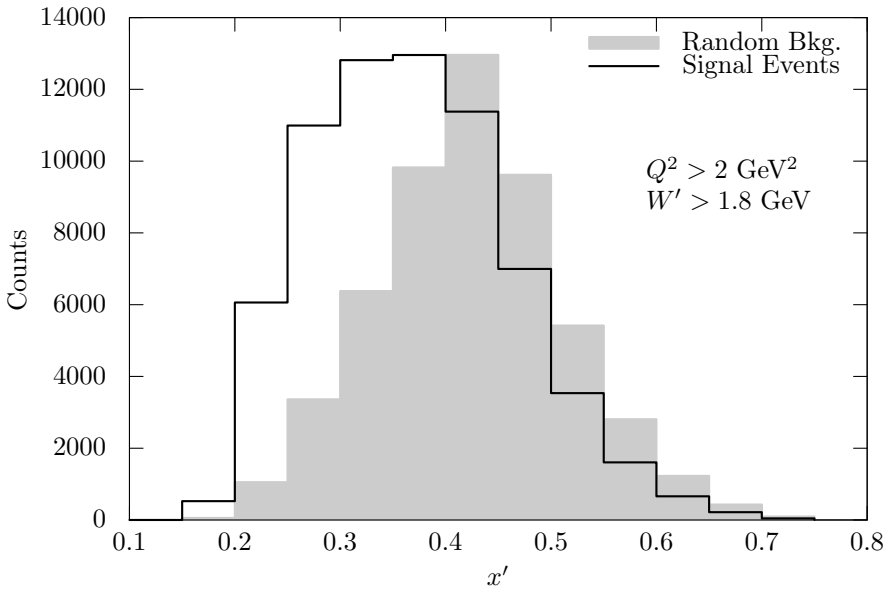

Figure 8: The distribution of reconstructed x'

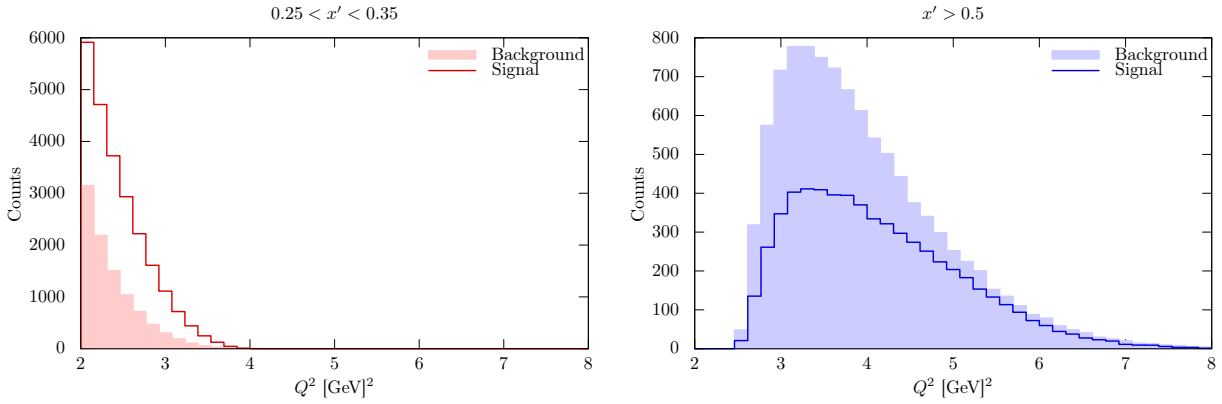

Figure 9: The distribution of reconstructed Q^2

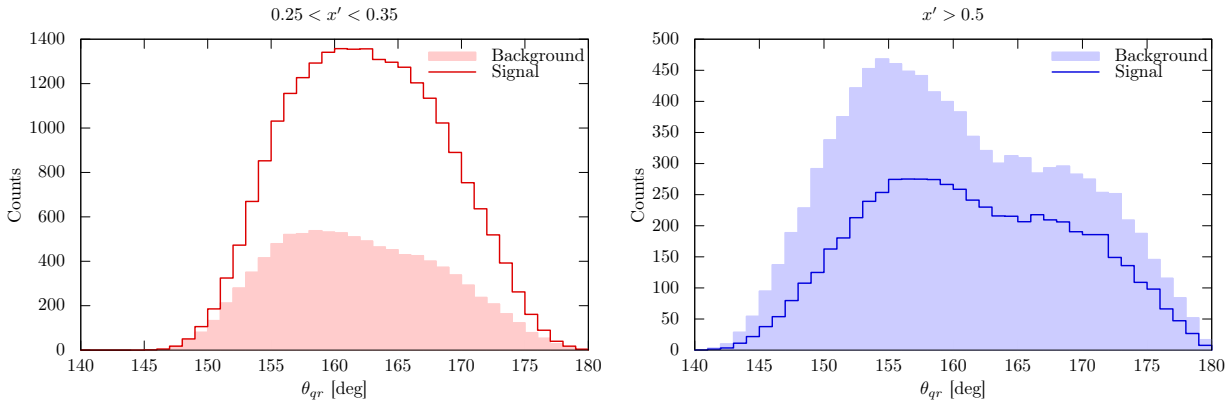

Figure 10: The distribution of reconstructed θ_{qr}

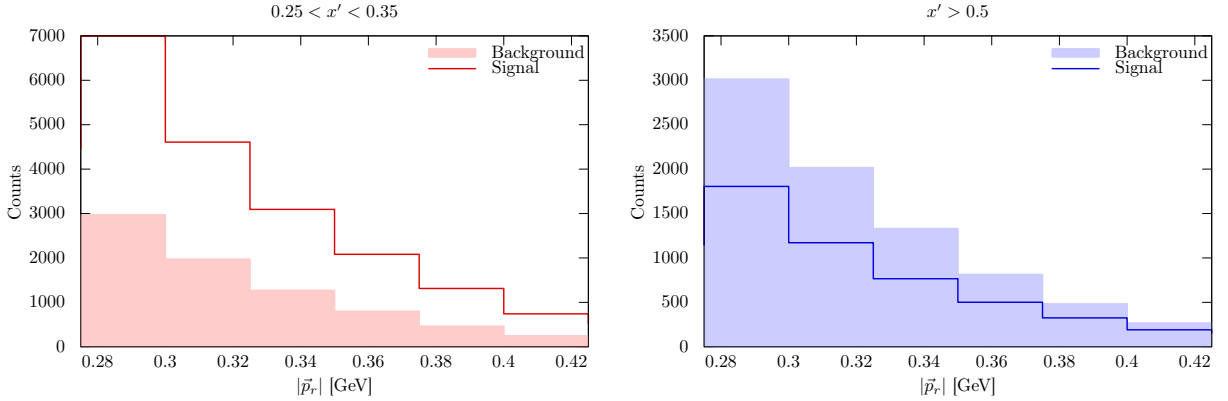

Figure 11: The distribution of reconstructed $|\vec{p}_r|$

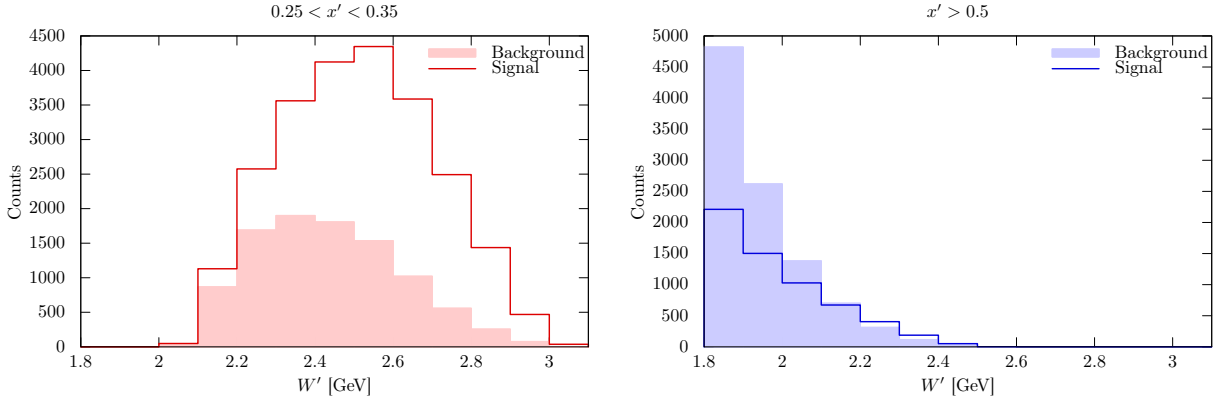

Figure 12: The distribution of reconstructed W'

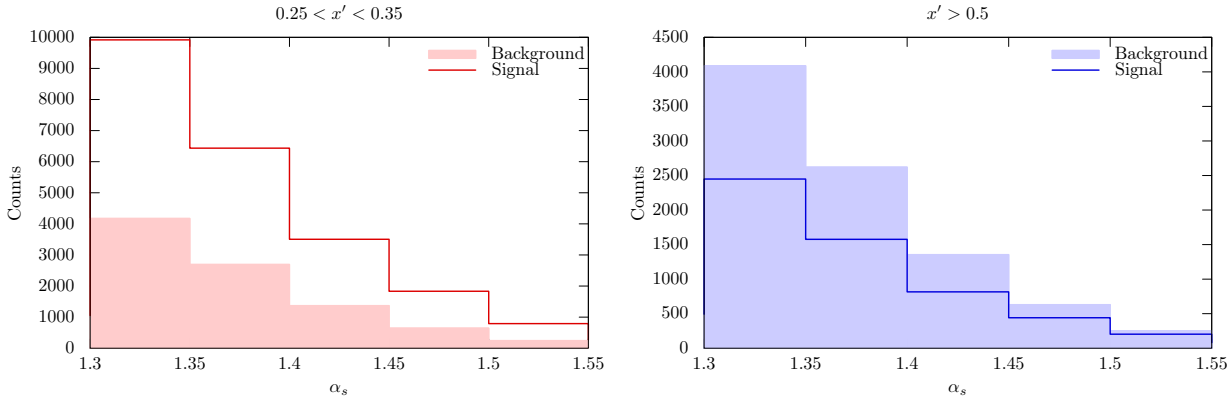

Figure 13: The distribution of reconstructed α_s

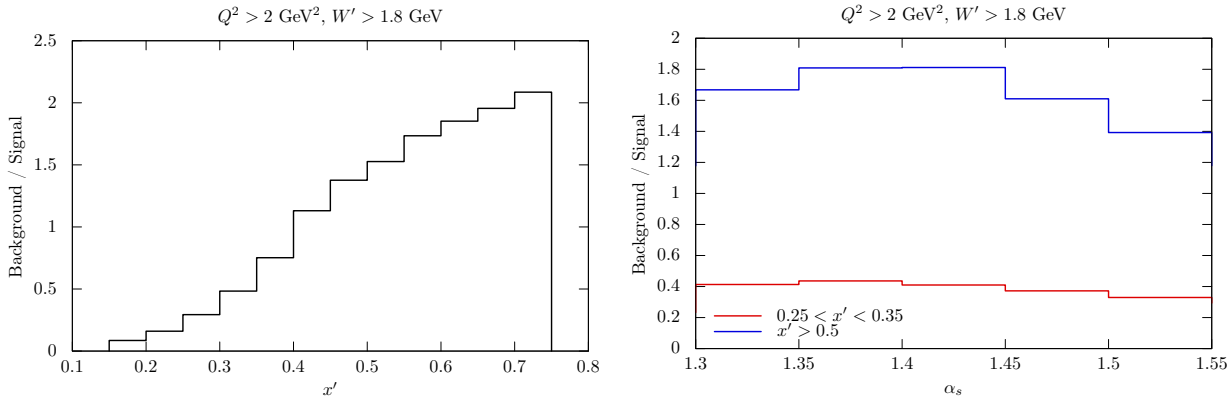

Figure 14: The ratio of background-to-signal is shown as a function of x' and α_s.

	$0.25 < x' < 0.35$			$x' > 0.5$		
Bin	Signal	Background	δSignal	Signal	Background	δSignal
$1.30 < \alpha_s < 1.35$	10100	4170	1.18%	2450	4090	3.30%
$1.35 < \alpha_s < 1.40$	6180	2690	1.52%	1450	2620	4.40%
$1.40 < \alpha_s < 1.45$	3340	1370	2.05%	748	1350	6.13%
$1.45 < \alpha_s < 1.50$	1730	645	2.81%	391	630	8.17%
$1.50 < \alpha_s < 1.55$	742	244	4.23%	181	252	11.5%

Table 1: The expected number of signal and background counts in five α_s bins (taken from figure 13) as well as the expected statistical precision of the signal rate (estimated from equation 11)

4.1 Statistical Power

The statistical precision with which the signal rate in a bin can be measured depends on both the number of signal counts S and the number of background counts B. The uncertainty on the total number of counts will be, from the Poisson distribution, $\sqrt{S+B}$. We can assume that the background rate can be determined with very precision from the "off-time" singles rates, and therefore subtracted. Thus, the fractional uncertainty in a bin can be estimated with:

$$\frac{\delta S}{S} = \frac{\sqrt{S+B}}{S}. \tag{11}$$

Table 1 lists the expected signal and background counts in five α_s bins for both the low x' and high x' kinematics. The data were previously shown in figure 13. In addition, the expected relative statistical power for the determination of the signal countrates is given, calculated using equation 11. This table can compared to table 2 of the BAND proposal. By extending the W' limit down to 1.8 GeV, the statistical power for the high x' kinematics is significantly increased (a factor of 2 for the highest α_s bin) while only slightly worsening the statistical power in low x' kinematics.

5 Resolution

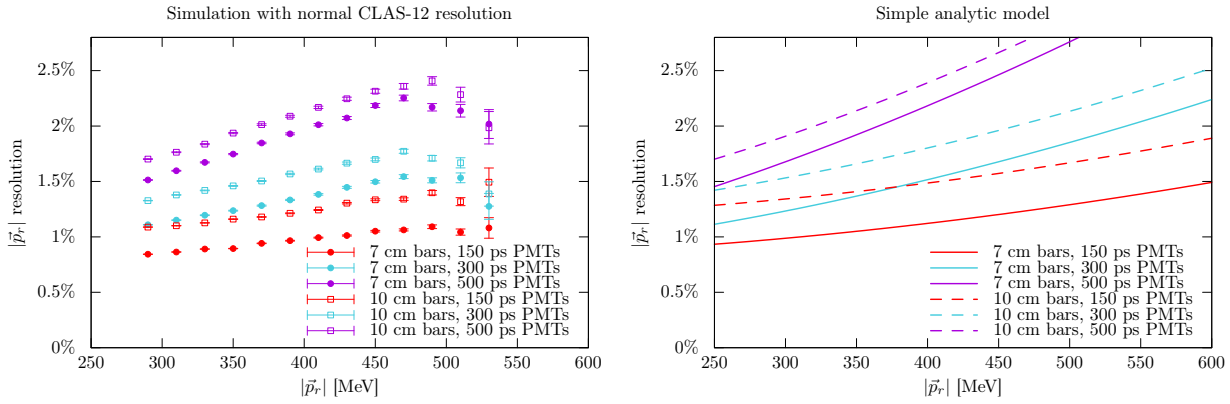

Figure 15: The resolution for reconstructing $|\vec{p}_r|$ for different bar widths and PMT resolutions is shown. The left figure shows the results of the simulation. The right figure shows the prediction from a simple analytic model (equation 12).

To study the resolutions, I simulated events, smeared the reconstructed positions and times as described in section 2, produced reconstructed kinematic values. I produced histograms of the difference between the reconstructed and true values and then fit these histograms with a simple Gaussian in order to extract resolutions. I will begin this section with a discussion of the resolution for reconstructing p_r, since it can be

calculated analytically with a few approximations. Since

$$\frac{\partial p_r}{\partial t_{\text{flight}}} = \frac{p_r^2 E_r c}{m_n^2 z}$$

and since

$$\frac{\partial p_r}{\partial z} = \frac{p_r E_r^2}{m_n^2 z}$$

then we can approximate the resolution with the expression:

$$\frac{\delta p_r}{p_r} = \frac{1}{m_n^2 z}\sqrt{p_r^2 E_r^2 c^2 \left(\frac{\sigma_t^2}{2}\right) + E_r^4 \left(\frac{W^2}{12}\right)}, \tag{12}$$

where σ_t is the PMT resolution and W is the bar width. This expression neglects the change in reconstructed flight path due to changes in the reconstructed transverse position, but it is simple and analytic, and can be used as a baseline for comparison. Figure 15 shows a side-by-side comparison of the resolution found from the simulation (left) and the resolution predicted by equation 12. The simulation confirms the over overall scale, and confirms the relative change in resolution due to increasing the bar width or the PMT resolution.

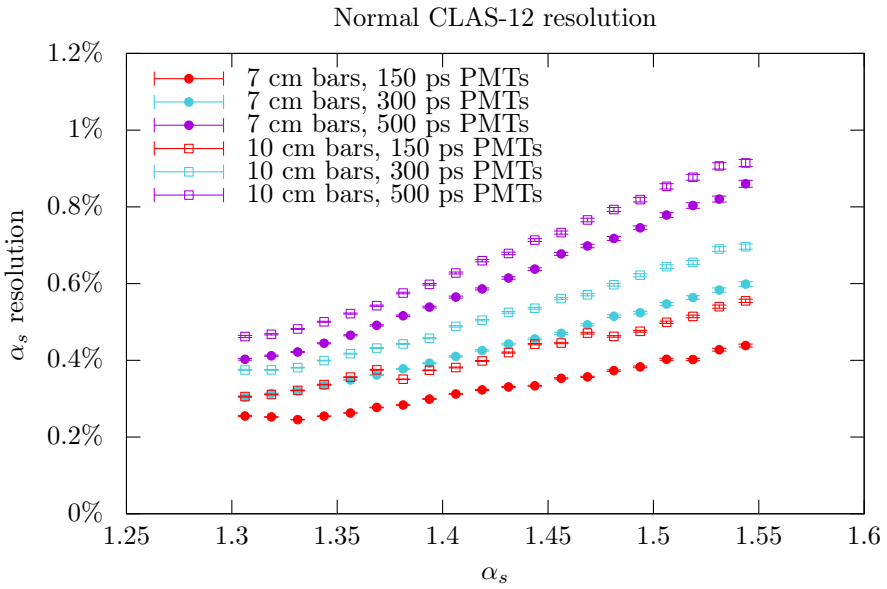

Figure 16: The resolution for reconstructing α_s for various bar width and PMT resolutions.

Figure 16 shows the resolution for reconstructing α_s, given normal CLAS12 resolution. The bar width and PMT resolution have a slight effect on the resolution, and even in a 10 cm/500 ps scenario, the resolution never exceeds 1%.

Figures 17, 18, 19, and 20 show W' and x' resolutions as functions of true W' and true x'. The distributions of of the difference between reconstructed and true values were sufficiently Gaussian to allow stable Gaussian fits to determine the distribution widths.

Figure 17 shows the effect of changing the width of the individual BAND scintillator bars. Since there is a change in resolution with changing α_s, I have limited this study to events with $1.3 < \alpha_s < 1.35$. I initially simulated bars with widths of 7 cm, 8 cm, 9 cm, and 10 cm, but since I could barely see any difference between the results, I added a simulation where BAND was built from one 40 cm wide bar, just to prove that the simulation was working. As can be seen, the 40 cm bar has significantly worse resolution, but it is not outrageously poor. In fact, the width of the bar seems not to have a large impact on our ability to reconstruct W' and x'.

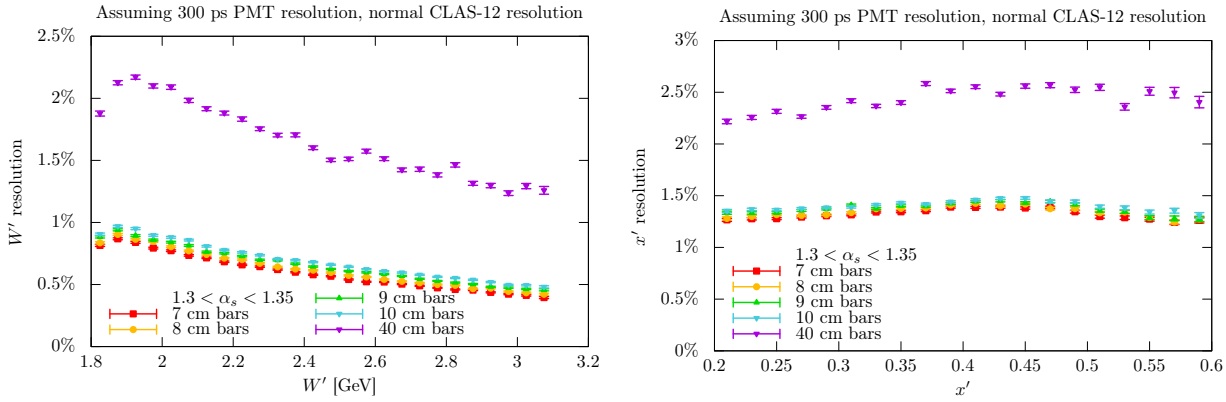

Figure 17: The effect of bar width on W' and x' resolution.

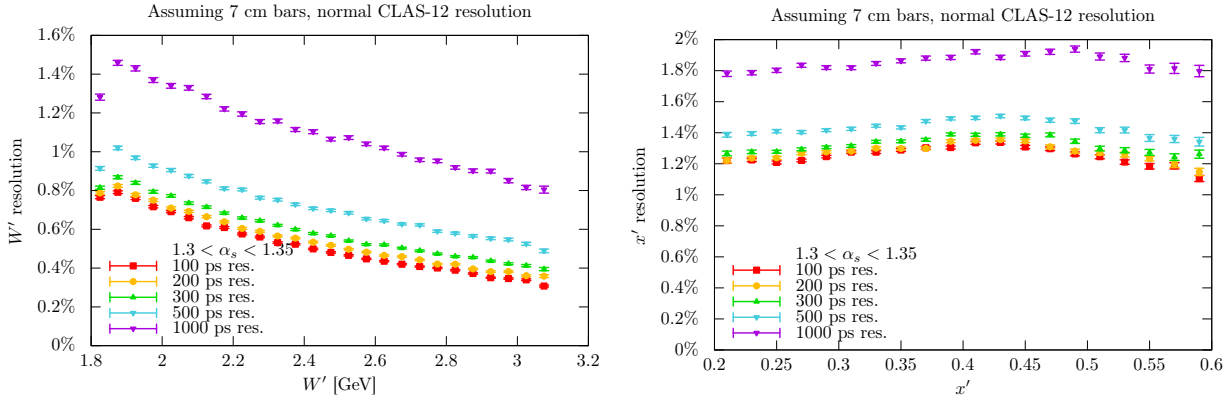

Figure 18: The effect of PMT time resolution on W' and x' resolution.

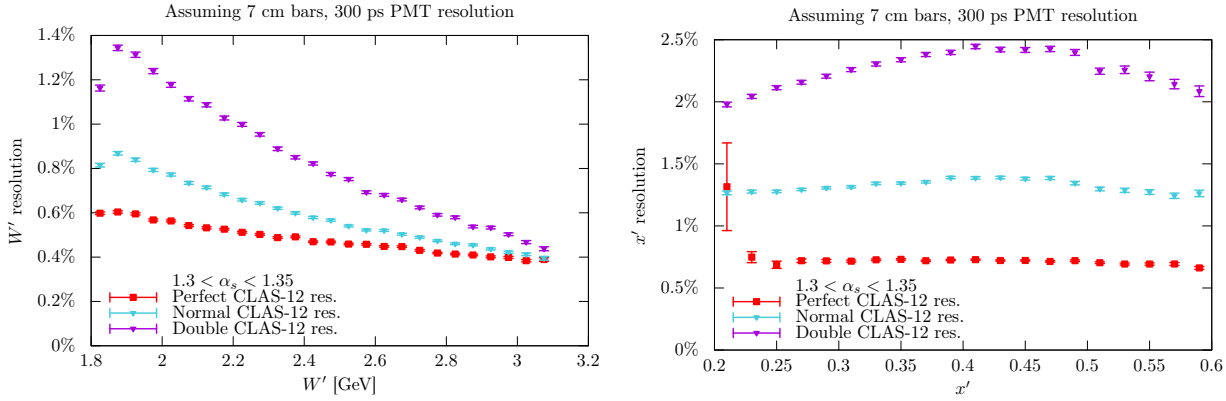

Figure 19: The effect of CLAS12 resolution on W' and x' resolution.

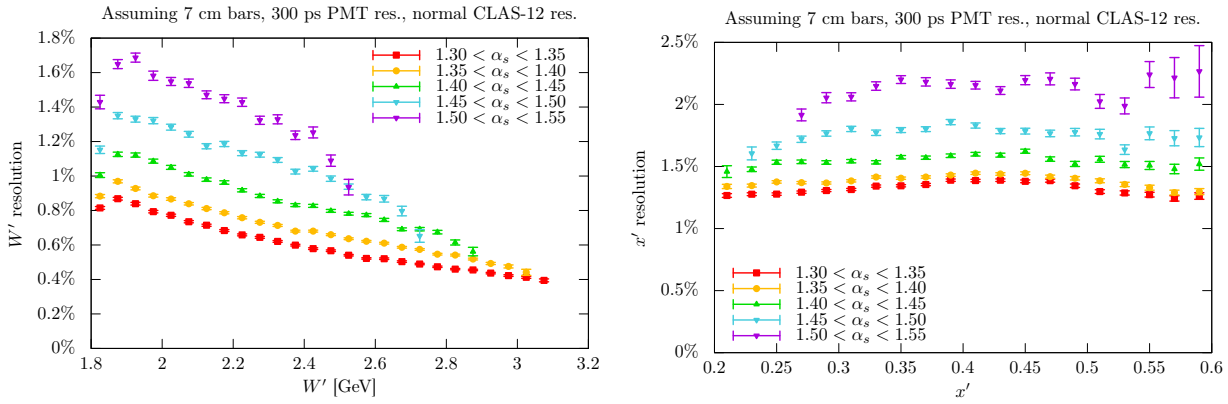

Figure 20: The change in resolution in different α_s bins.

Figure 18 shows the effect of changing PMT resolution. As before, α_s is restricted to $1.3 < \alpha_s < 1.35$. The PMT resolution can make a slight change in the reconstruction of W' and x', but for reasonable PMTs, we can expect no worse than 1% resolution for W' and 1.4% resolution for x' in this particular α_s bin.

Figure 19 shows how the CLAS12 spectrometer can affect the resolution. Making the CLAS12 resolution a factor of two worse, makes the reconstructed W' and x' resolutions approximately worse by a factor of two. This indicates that the resolution for W' and x' is largely driven by the CLAS12 performance. The red points in figure 19 show the reconstruction resolution assuming perfect electron reconstruction, i.e., zero CLAS12 resolution. These points set the scale for the resolution effects due to BAND.

Figure 20 shows the resolution for different bins in α_s. This plot essentially proves the point that α_s must be fixed when considering resolutions. The resolution for the highest α_s bin is worse by over a factor of two.

6 Bin Migration

The limit of what detector resolution we can tolerate is determined by the systematic uncertainty coming from bin migration. Given non-zero resolution, the reconstructed event rate in a bin will be slightly different from the true event rate. Some number of events truly beloning to the bin will be reconstructed as being outside of the bin (the loss fraction), while some number of events from outside the bin will be falsely reconstructed inside the bin (the contamination fraction). While a correction (determined from simulation) can be applied, the uncertainty on that correction will remain as a systematic uncertainty on the measured event rate. If the amount of bin migration can be diminished, the systematic uncertainty on the measurement will be correspondingly reduced.

To estimate the effect on bin migration, I imagine an analysis with five bins in α_s (ranging from 1.3 to 1.55) and five bins in x' (ranging from 0.15 to 0.65). I compare the generated and reconstructed values of x' and α_s and, for each bin, look at:

1. Contamination Fraction: $C \equiv N^{\text{gen. outside}}_{\text{recon. inside}}/N_{\text{recon. inside}}$
2. Loss Fraction: $L \equiv N^{\text{recon. outside}}_{\text{gen. inside}}/N_{\text{gen. inside}}$
3. Change in yield: $\Delta N/N \equiv (N_{\text{recon. inside}} - N_{\text{gen. inside}})/N_{\text{gen. inside}}$

A correction can be made for the change in yield using simulation. However, the uncertainty on that correction depends on the magnitude of the contamination fraction and loss fraction. One can have much greater confidence correcting for a small amount of contamination and loss than for large amounts, even if the changes in yield are identical.

Statistical precision is an important part of this optimization; there is no value in expending resources to reduce the systematic uncertainty far below the limit of the statistical uncertainty. As a benchmark, Figure 21 shows the estimated statistical precision of each bin in this particular 25-bin analysis taking background

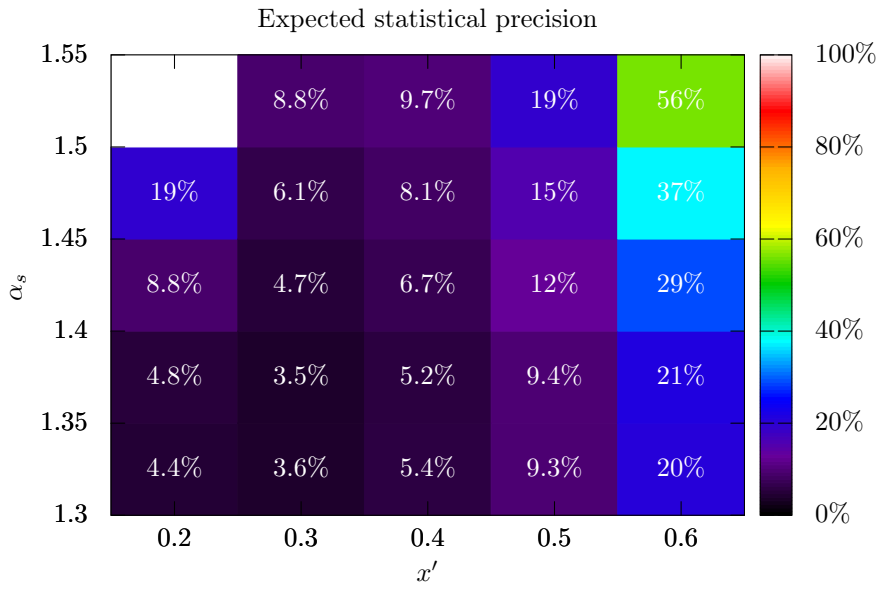

Figure 21: There is little to be gained by reducing the systematic uncertainty far below the expected statistical precision.

rates into account. For comparison, in this section, I use a simple estimate of the systematic uncertainty due to bin migration:

$$\frac{\sigma_{\text{sys.}}}{N} = 20\% \times \sqrt{C^2 + L^2}, \tag{13}$$

i.e., that the systematic error can be conservatively estimated as 20% of the contamination and loss fractions added in quadrature. By comparing this to the statistical uncertainty, the effectiveness of different BAND configurations can be judged. In an effort to make this judgement safely conservative, I used "double" CLAS12 resolution in the following simulations.

To start, let's first consider an unrealistic scenario of "double" CLAS12 resolution, combined with perfect BAND resolution, i.e., BAND reconstructs neutron momentum vectors with perfect accuracy. This scenario sets a lower limit for the smallest migration that can be achieved by optimizing the BAND detector design. Figure 22 shows four plots. The top left shows the contamination fraction, the top right shows the loss fraction. These are nearly equal, and the result is that the change in yield (bottom left) is very close to zero. The bottom right shows my simple estimate of systematic uncertainty due to bin migration relative to the expected statistical uncertainty. In this scenario, and given this 25 bin analysis, we can expect migration of approximately 5–10% in and 5–10% out. It is unrealistic to aim for better than this limit. Furthermore, the expected systematic uncertainty is well less than the statistical uncertainty in all bins, so there is little benefit to achieving this level of performance.

Compare figure 22 to figure 23, the bin migration in a pessimistic scenario: 10 cm bars and 500 ps PMTs. Since this design is easily achievable, this represents a worst-case scenario for bin migration. The net migration is still very small, but the contamination and loss range from 15–30%. Still, the systematic uncertainty is still smaller than the statistical uncertainty in most of the bins, and is only larger in a few of the high-precision bins for which $x' = 0.3$'. From this, we can see that the resolutions associated with 10 cm bars and 500 ps PMTs would not compromise the experiment.

For further comparison, figure 24, 25 and 26 show the migration scenarios for 10 cm bars with 300 ps PMTs, 7 cm bars with 500 ps PMTs, and 7 cm bars with 300 ps PMTs respectively. These scenarios fall in between the best (figure 22) and worst (figure 23) cases.

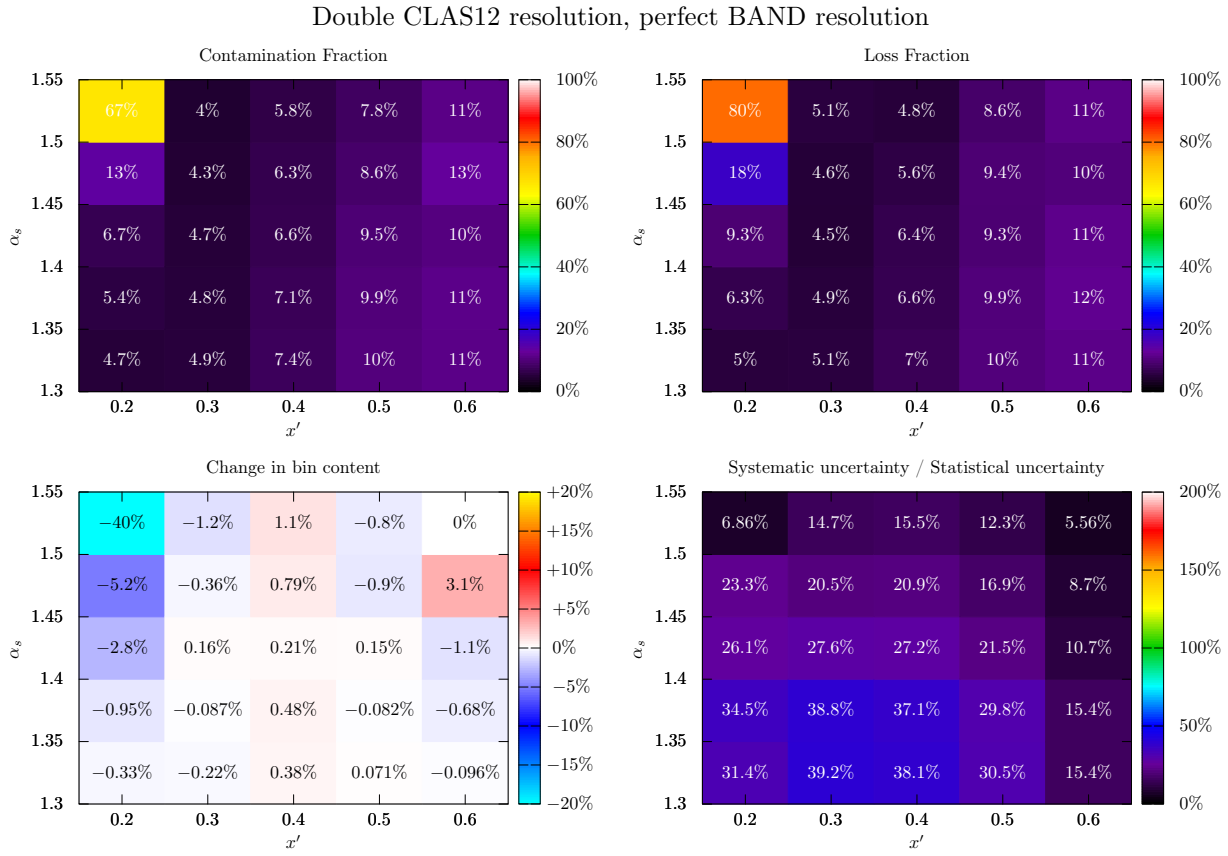

Figure 22: The combination of "double" CLAS12 resolution and perfect BAND resolution sets the floor for the lowest achievable bin migration that can be achieved by optimizing the BAND design.

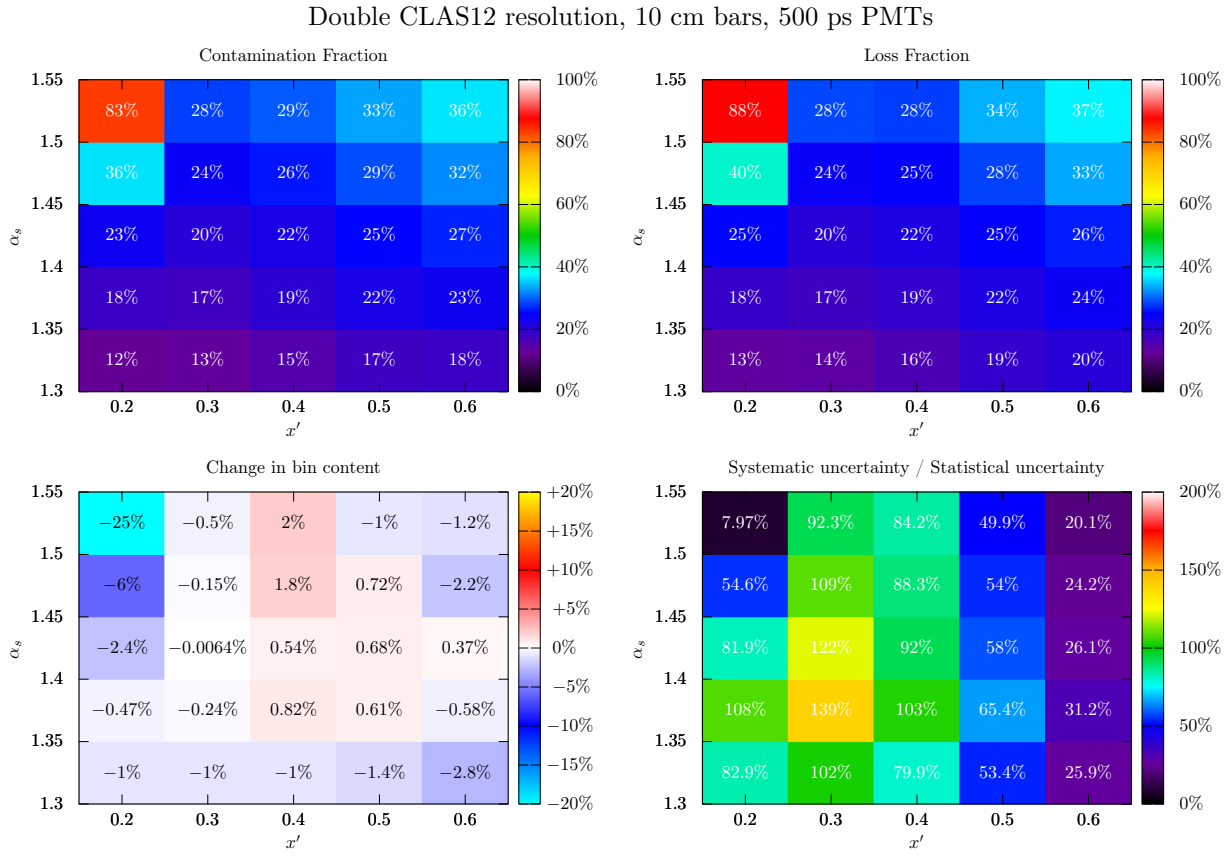

Figure 23: A scenario with 10 cm bars, 500 ps PMTs, and "double" CLAS12 resolution represents a worst case bin migration scenario.

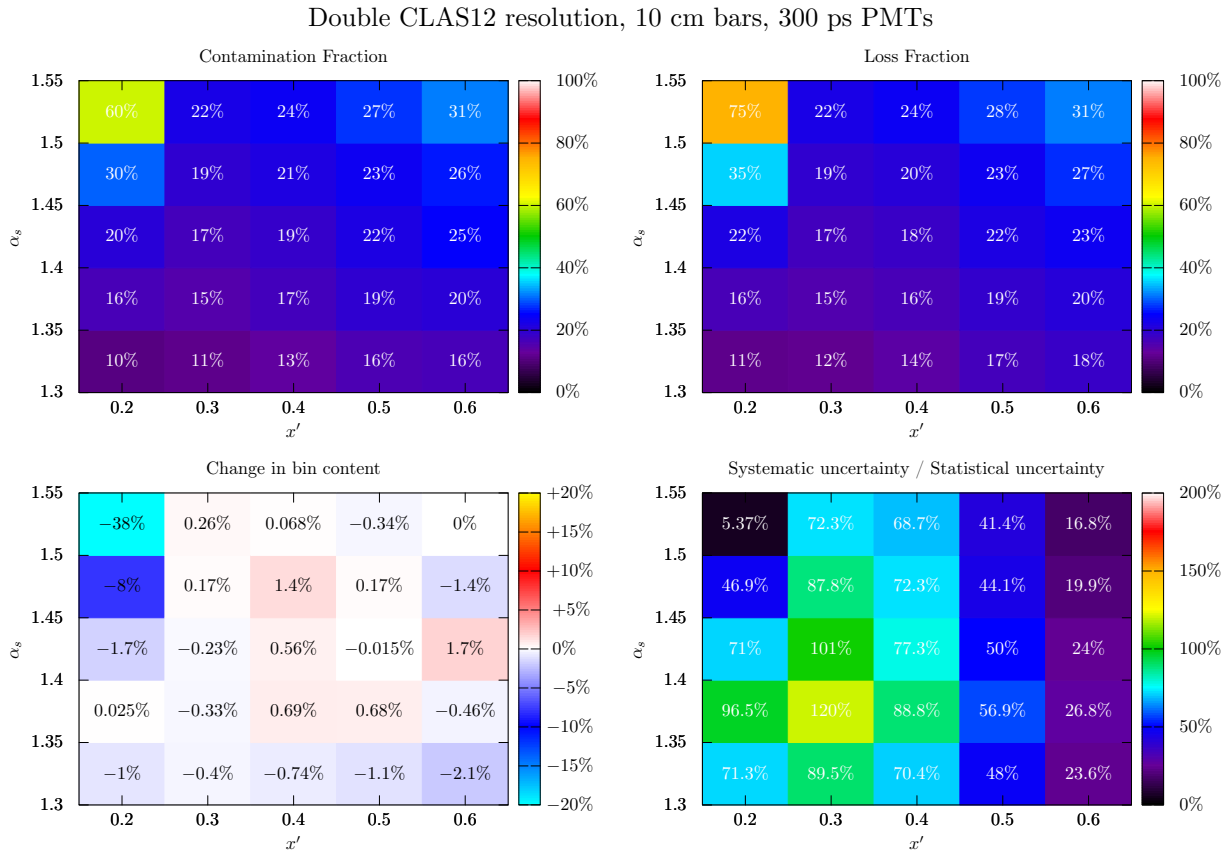

Figure 24: A scenario with 10 cm bars, 300 ps PMTs, and "double" CLAS12 resolution.

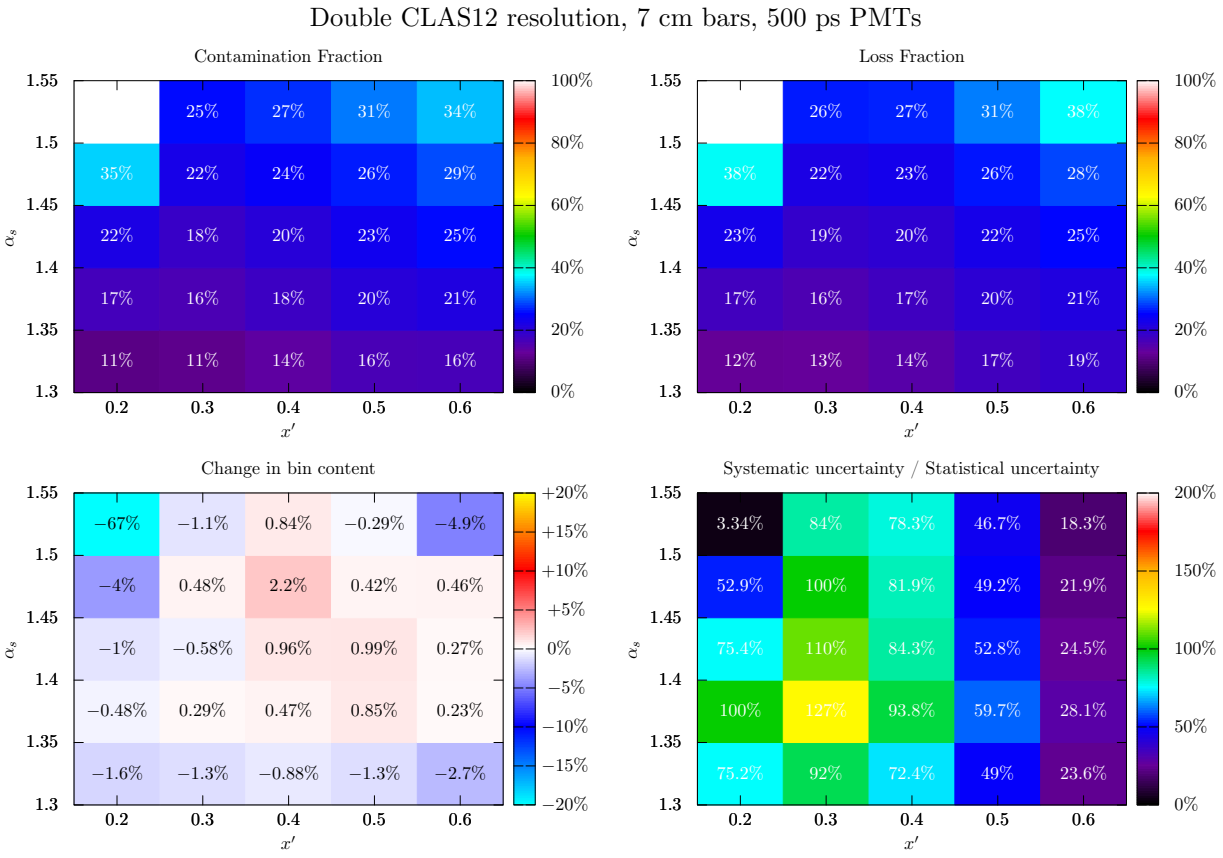

Figure 25: A scenario with 7 cm bars, 500 ps PMTs, and "double" CLAS12 resolution.

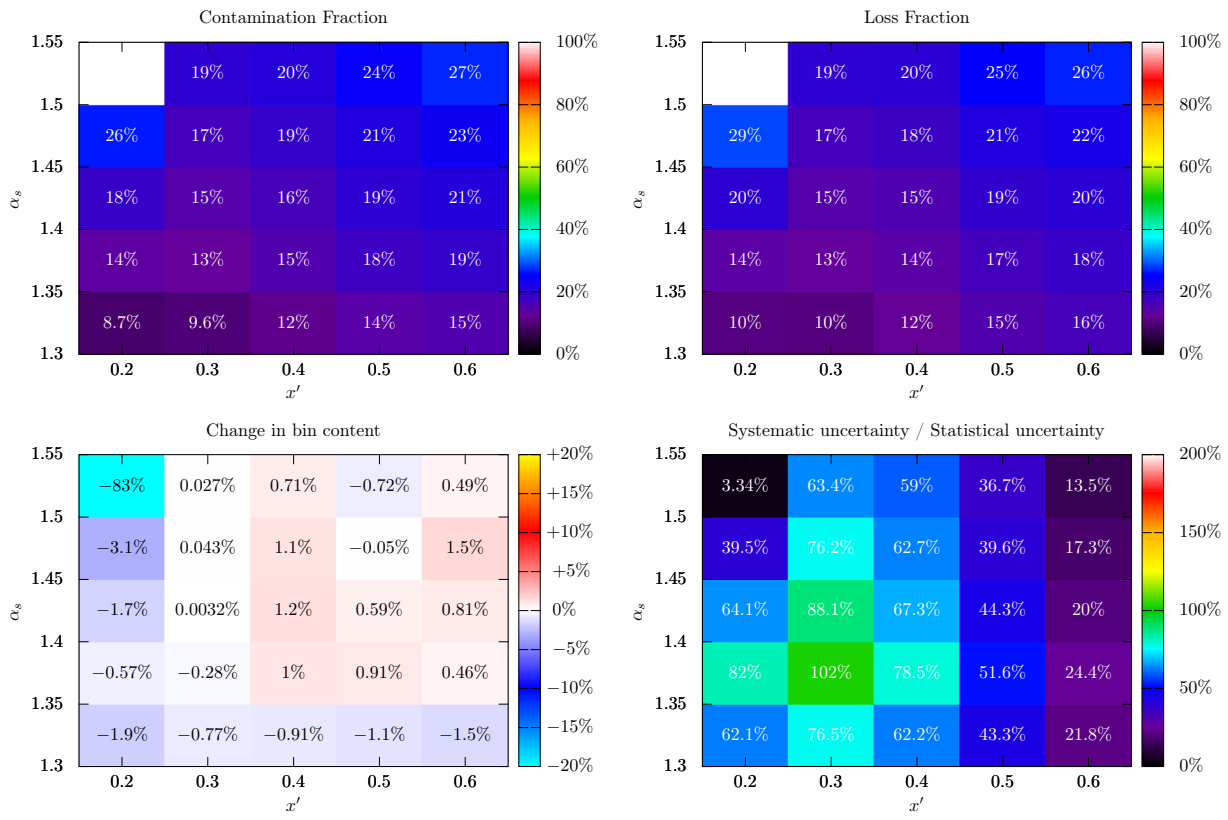

Figure 26: A scenario with 7 cm bars, 300 ps PMTs, and "double" CLAS12 resolution

.

7 Conclusions

This report shows estimates that can be made using the BAND Monte Carlo simulation in its current state. This simulation will be made more sophisticated and these estimates will continue to be refined. In particular, studies are needed to optimize the experiment's energy threshold. However, there are several conclusions that can be drawn from this study:

1. A 3-dimensional simulation produces only slight changes in the distributions of kinematic variables, and any drop in rate can be compensated by reducing the W' threshold from 2 GeV to 1.8 GeV.
2. We should expect a background rate that is between 1.5 and 2 times the signal rate for high-x' events.
3. Bar width does not significantly affect BAND performance.
4. 10 cm bars and 500 ps PMTs will be adequate.

References

[1] L. Weinstein *et al.*, *In Medium Proton Structure Functions, SRC, and the EMC effect.* Hall-B Proposal, April 2015.

[2] M. Mestayer *et al.*, *CLAS12 Drift Chambers (DC).* DC Group, February 2016. `https://www.jlab.org/Hall-B/clas12-web/specs/dc.pdf`.